

Flow Control of Transonic Airfoils using Optimum Suction and Injection Parameters

Z. Seifollahi Moghadam and A. Jahangirian[†]

Department of Aerospace Engineering, Amirkabir University of Technology, Tehran, 15875-4413, Iran

[†]Corresponding Author Email: ajahan@aut.ac.ir

(Received February 11, 2015; accepted August 24, 2016)

ABSTRACT

In this paper, the application of the surface mass transfer optimization in shock wave-boundary layer interaction control at off-design conditions of transonic aircraft wing is presented. The suction or injection parameters include for example its position on the airfoil, its angle, the length of the hole and the rate of the injected or sucked flow. The optimization process is carried out using an efficient Genetic Algorithm (GA) method. The compressible viscous flow equations in Reynolds Averaged form are solved together with a two-equation k-epsilon turbulence model to accurately compute the objective function. Four different objective functions are introduced including maximum lift to drag ratio, minimum drag coefficient, maximum lift to drag ratio with no drag increment and minimum drag coefficient with no lift decrement. Effectiveness of each objective function is examined by comparing the optimum results in terms of the flow control parameters and flow characteristics.

Keywords: Aerodynamic optimization; Genetic Algorithm; Surface mass transfer; Transonic flow control; off-design conditions.

NOMENCLATURE

C_d	drag coefficient	Re	Reynolds number
C_f	skin friction coefficient	t	time
C_L	lift coefficient	u, v	Cartesian mean-velocity components
C_p	pressure coefficient	y^+	surface non-dimensional normal distance
C_Q	suction/injection coefficient	α	angle of attack
c	airfoil chord	Δt	time step
D	artificial dissipation terms	ε	dissipation rate of turbulent kinetic energy
F, G	Cartesian components of convective fluxes	η	order of grid nodes in vertical direction
k	turbulent kinetic energy	μ	molecular viscosity
M	Mach number	ξ	order of grid nodes in horizontal direction
p	static pressure	ρ	density
Q	array containing the conserved variables	Ω	cell area
R	array of residuals		

1. INTRODUCTION

The interaction of shock waves with boundary layers in transonic and high subsonic regimes is of great importance due to the fact that this basic phenomena leads to extremely undesirable effects, such as drag rise, massive flow separation, shock unsteadiness and aerodynamic performance losses.

Shock wave control for large flight vehicles at cruise conditions can cause extensive drag reduction and aerodynamic performance increase, so that it reduces fuel consumption and increases flight range. There are a wide range of studies dedicated to the area of shock waves creation, their interaction with boundary layer and their control (Babinsky and Harvey 2011, Stanewsky *et al.*

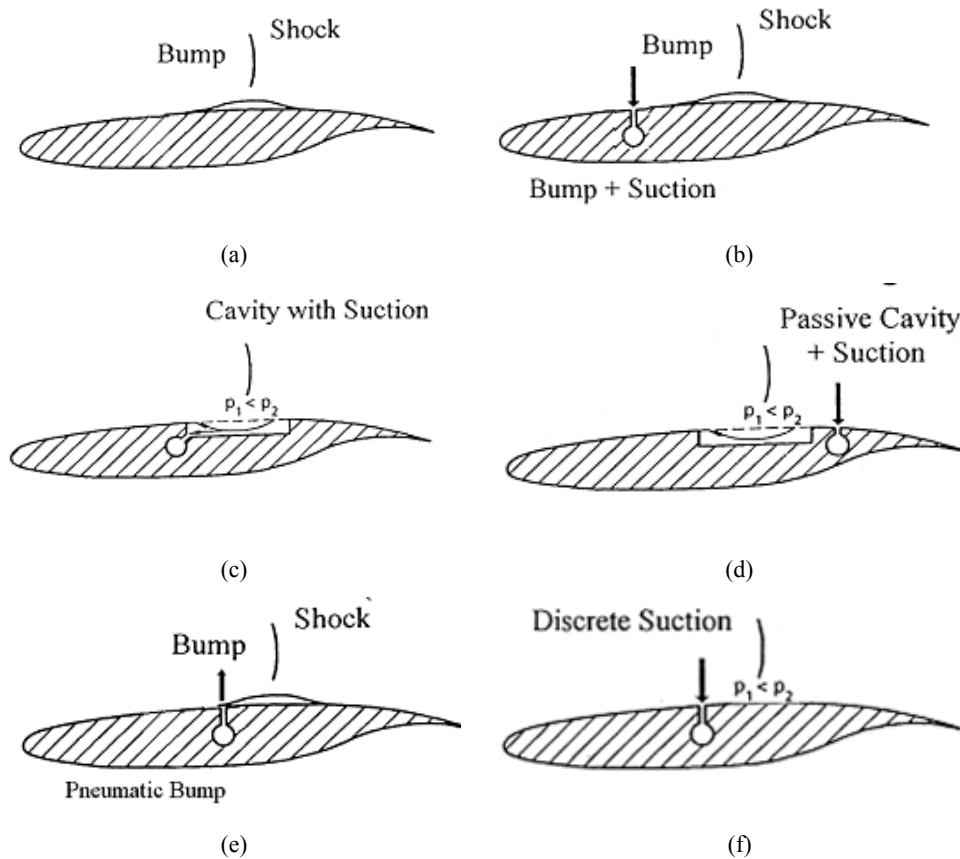


Fig. 1. Euroshock presented methods to reduce shock wave related drag.

2002). It should be mentioned that although wave drag contribution in comparison with skin friction and induced drag is normally low for well-designed transonic flight vehicles, but due to the fact that the flight of these vehicles is very close to drag divergence Mach number, with small increment in velocity, shock wave drag contribution increases very sharply. In addition, the change of shock wave location as a result of flow control device can change the lift coefficient value significantly. Thus, efficient tuning of the flow control device is of great importance and is not a vital task.

Several passive and active methods for control of the shock wave and boundary layer interaction and its resultant drag reduction have been presented (Khoshkhoo and Jahangirian 2016). The general presented methods in Euro-shock project (Stanewsky *et al.* 2002) in the area of shock waves drag reduction is illustrated in Fig. 1. These methods include using a bump to control shock wave, hybrid control of bump and upstream suction, cavity ventilation with downstream suction, passive cavity with inside suction, pneumatic bump and discrete suction upstream of the shock wave.

One can use pressure difference across the shock to create a flow circulation (Delery 1999). This can be done by using a cavity and perforated plate in the shock wave location. Experimental tests show that pressure increase upstream the shock wave results in noticeable decrease in wave drag, although total

drag increases due to increase in skin friction in control position. By the appointment of suction behind the cavity, boundary layer is thinned and the obtained results are more favorable (Stanewsky *et al.* 2002).

Two main active methods include surface mass transfer and local surface modification. The latter could be achieved by applying a set of actuators which could deform the flexible skin of the wing. The main objective of this method and pneumatic bump or surface flow injection is changing the slope of the local surface near the location of the shock wave that creates the isentropic compression waves and thus making a condition for Mach decrement of flow upstream the shock wave. Downstream the shock wave, the flow becomes subsonic via a weakened shock wave (Stanewsky *et al.* 2002, Qin *et al.* 2002). Mass injection for control of shock wave has been investigated by Wong (1977) experimentally.

It is notable that making suction upstream the shock wave doesn't show positive effect on the wave drag decrement and can increase the shock wave strength instead. However, because this method has the potential to control boundary layer growth in encountering shock wave, by the reduction in viscous drag, it can decrease total drag when shock wave appears on the wing. The hybrid control of bump and upstream suction has the advantage of boundary layer thinning; hence after the bump

position and shock wave occurrence, viscous losses resulting from boundary layer growth and separation will be reduced (Stanewsky *et al.* 2002). Smith and Walker results (1960) show that by the strong suction in the interaction region, lift will be increased, because the separated flow in shock-boundary layer interaction region will be sucked in. Although with suction, the boundary layer is thinner, but the shock wave is more stable and normal and thus its strength will be increased which results in wave drag increment also. This can be noticed in numerical studies of Qin *et al.* (1998) whom parametric studies show that suction generally promotes airfoil aerodynamic performance by increasing the lift to drag ratio. While it increases the shock wave strength and leads it to the downstream. Despite the fact that with the active flow control, some degrees of improvement in performance is obtainable, aerodynamic performance sensitivity to design parameters makes the problem more significant, so that the thorough study of all parameters is computationally expensive. Consequently, the designer must keep in mind the optimization of several parameters. In continue, with the purpose of more flexible active flow control, an automatic optimization process is needed.

Genetic Algorithm is one of the stochastic methods, which has been widely used in aerodynamic design. This algorithm doesn't need objective function derivatives and just uses the evaluation of decision variables (Jahangirian and Shahrokhi 2009, Goldberg 1989). It uses a set of coded decision variables that have the potential to be the problem answer, and could start search process in parallel. This algorithm uses statistics rules for governing search direction and uses random searching for gaining a better search space. More information about GA can be found in (Deb 2001). By the consideration of aerodynamic optimization difficulties such as nonlinear nature of the governing equations and thus the uneven distribution of objective function with respect to decision variables (Obayashi and Tsukahara 1997), large numbers of decision variables in objective function space (Oyama *et al.* 2001), complicated interaction between flow solver and optimization equations (Anderson and Bonhaus 1999), GA has been selected for the optimization in this research. Marco and Lanteri (2000) used a parallel GA to reduce computation costs in airfoil optimum design. Zhang *et al.* (2002) optimized airfoil and wing in subsonic and transonic regime by the implementation of GA. Jahangirian and Shahrokhi (2011) employed GA to optimize airfoil aerodynamic performance using CFD techniques. They also presented a fast method for aerodynamic optimization of transonic airfoil by means of GA and neural networks (Shahrokhi and Jahangirian 2010).

Yagiz and Kandil (2009) have optimized the suction and injection transonic flow control parameters using a gradient based method. The location of the surface mass transfer was limited to three fixed positions in the aforementioned article. As another

example of the latest researches in the area of the active flow control optimization through surface mass transfer, one can mention the study of Pehlivanlou and Yagiz (2012) in which by the use of a surrogate based Genetic Algorithm, the strength and the angle of the mass transfer were optimized. However, the position of mass transfer is considered to be fixed in this research. Yagiz and Kandil (2012) also studied the possibility of wave drag minimization using contour bump or jet actuator or hybrid control. The optimization method is gradient-based in this study. Moreover, in a recent study by Mazaheri and Nejati (2016) the optimization of contour bump together with suction and blowing has been carried out using a gradient-based adjoint algorithm.

The main purpose of the current study is the optimization of the active flow control by means of the surface mass transfer at off design conditions in which the vehicle drag encountered a sudden increment. The control parameters here include the position, strength and the angle of the suction or injection.

2. FLOW SOLUTION ALGORITHM

The following section outlines flow solution algorithm including time and space discretization of flow equations and mesh generation scheme.

2.1 Governing Flow Equations

The huge numbers of airfoil flows with different surface mass transfer parameters that are generated by the GA are evaluated based on the numerical solution of the governing flow equations. The physical problem under consideration is that of compressible viscous flow. The mathematical model used is the two-dimensional compressible Navier-Stokes equations. In turbulent cases, the Reynolds averaged Navier-Stokes equations are used. The computational method applied to solve the problem of surface mass transfer is what is developed in (Stolcis and Johnston 1990, Jahangirian and Hadidoolabi 2005). The conservative form of two dimensional unsteady compressible Navier-Stokes equations is:

$$\frac{\partial Q}{\partial t} + \frac{\partial F}{\partial x} + \frac{\partial G}{\partial y} = 0 \quad (1)$$

Where Q is the array containing the mean flow conserved variables and F and G contain the Cartesian components of the flux vector which include convective and viscous fluxes:

$$F = F^I - F^V, \quad G = G^I - G^V \quad (2)$$

Superscripts I and V are used to separate inviscid and viscous terms. The finite-volume method applied to the governing mean-flow equations in integral conservation form can be obtained by integrating the governing equations over the domain of interest Ω and applying the Gauss theorem to the second term of equation:

$$\frac{d}{dt}(Q_i A_i) + R_i(Q) - D_i(Q) = 0 \quad (3)$$

A_i is the area of the cell i . The artificial dissipation fluxes $D_i(Q)$ consists of a blending of a second order term to diminish oscillation around discontinuities such as shock wave and a forth order term to damp high oscillations in domain. It is added due to the central difference nature of our discretization. In order to get a fully implicit method the Eq. (3) could be rewritten as:

$$\frac{d}{dt}(A_i Q_i) + R_i(Q^{n+1}) - D_i(Q^{n+1}) = 0 \quad (4)$$

where superscript $n+1$ shows the time step $(n+1)\Delta t$ and d/dt has been modeled using an implicit second order backward difference so that:

$$\begin{aligned} & \frac{3}{2\Delta t}(A_i^{n+1} Q_i^{n+1}) - \frac{2}{\Delta t}(A_i^n Q_i^n) + \\ & \frac{1}{2\Delta t}(A_i^{n-1} Q_i^{n-1}) + R_i(Q^{n+1}) - D_i(Q^{n+1}) = 0 \end{aligned} \quad (5)$$

Equation (5) for Q_i^{n+1} is a system of non-linear differential equations and cannot be solved with analytical methods. In this step by the definition of unsteady residual R^* as:

$$\begin{aligned} R_i^*(Q^{n+1}) = & R_i(Q^{n+1}) - D_i(Q^{n+1}) + \\ & A_i \left[\frac{3}{2\Delta t}(Q_i^{n+1}) - \frac{2}{\Delta t}(Q_i^n) + \frac{1}{2\Delta t}(Q_i^{n-1}) \right] = 0 \end{aligned} \quad (6)$$

and writing the differential equation with respect to imaginary time τ that the above equation is its steady state answer:

$$A_i \frac{\partial Q_i^{n+1}}{\partial \tau} + R_i^*(Q^{n+1}) = 0 \quad (7)$$

One can integrate the above equation in imaginary time τ and obtain its steady state answer which is Eq. (5) answer in real time step. In this study the system of Eq. (7) has been integrated using four-step explicit method in imaginary time. In addition, because the steady state answer is required, all the convergence acceleration methods such as residual smoothing and local time stepping could be applied. These methods reduce the computational time. Further details about the method can be found in (Jahangirian and Hadidoolabi 2005).

Turbulence effects can be taken into account by using a suitable turbulence model. In this paper, two-equation k-epsilon turbulence model developed with Launder and Spalding (1974) has been applied. The wall-function approach is adopted to treat the near-wall region of the boundary layer (Stolcis and Johnston 1990, Jahangirian and Hadidoolabi 2005). In this approach the quantities of interest are evaluated as functions of mean-flow quantities according to the law-of-the-wall. This approach is computationally very efficient, since a highly-refined computational grid is not required in the

near-wall region.

2.2 Initial and Boundary Conditions

The initial conditions ($t=0$) applied in the present method consist of setting all the quantities equal to their free-stream values. The wall boundary condition is the no-slip condition, which states that at the wall the velocity is zero. On the part of airfoil with mass transfer, the velocity normal component is computed as:

$$u_N = \frac{C_Q \rho_\infty U_\infty c}{\sum_{L_{\text{mass transfer}}} \rho_w \Delta s} \quad (8)$$

where suction/injection coefficient C_Q is defined as:

$$C_Q = \frac{\dot{m}}{\rho_\infty U_\infty c} = \frac{1}{\rho_\infty U_\infty c} \int_{s_1}^{s_2} \rho_w v_w ds \quad (9)$$

In addition to the normal velocity component, the tangential component is determined by the suction/injection inclination angle which is in the range of 0 to 180 degree to the airfoil surface.

Positive C_Q coefficients indicate injection and negative amounts are indications of suction. Knowing normal and tangential velocity component, their corresponding values in Cartesian system are:

$$\begin{aligned} u &= -u_N \frac{\Delta y}{\Delta l} + u_T \frac{\Delta x}{\Delta l} \\ v &= u_N \frac{\Delta x}{\Delta l} + u_T \frac{\Delta y}{\Delta l} \end{aligned} \quad (10)$$

Moreover, on the locations of airfoil with surface mass transfer, turbulent flow quantities are set by knowing the wall velocity so that

$k_{\text{wall}} = 0.000025 \left(u_{\text{wall}}^2 + v_{\text{wall}}^2 \right)$ is the turbulent kinetic energy on these locations. It should be mentioned that on the airfoils surface with mass transfer, the wall function treatment is switched off.

Since the main interest of the present method is the computation of high Reynolds number compressible turbulent flows, and since the viscous effects are present only in the regions very far from the outer boundary, it is reasonable to apply the characteristic-based outer boundary conditions developed for inviscid flows.

2.3 Grid Generation

Due to the fact that this study includes large number of CFD calls, the generation of a grid with high speed of generation and numerical simulation is of great importance. One of the most well-known structured grid generation techniques is hyperbolic technique. With this method high quality orthogonal cells with time advantages is achievable. Hyperbolic equations for grid generation are obtained from two conditions of orthogonality and cell area variations. The equations obtained from the conditions mentioned above are (Thompson *et al.* 1999):

Table 1 An example of design variables

genes	Starting grid cell number	Total number of cells	Suction/ injection indicator	Mass transfer coefficient	inclination angle [rad]
values	140	2	-1	0.0003	2.894

$$\begin{aligned}
 X_{\xi} X_{\eta} + Y_{\xi} Y_{\eta} &= 0 \\
 X_{\xi} Y_{\eta} - X_{\eta} Y_{\xi} &= F(\xi, \eta)
 \end{aligned}
 \tag{11}$$

where the non-dimensional coordinates ξ and η are the locations of the nodes.

3. OPTIMIZATION WITH GENETIC ALGORITHM

GA consists of a set of parameters forming the procedure of optimum result searching. The main standard GA operators include selection, mutation and crossover. The commonly used GA parameters include population size, chromosome length, crossover probability, mutation probability and disturbance range. These parameters interact each other from their effect on GA point of view. Although increasing the number of population increases the probability to get the global optimum, but it could result in ineffective domain searching and thus a waste of time also. The population size considered in this study is 10. In real coding method of design variables, the chromosome length will be considered as five containing the location, length, strength, inclination angle and suction or injection nature of the mass transfer. An example of the design variables can be illustrated as Table 1:

In this chromosome the first gene (140) indicates the grid-cell number which is the starting location of mass transfer. The next gene (2) is the total number of cells where mass transfer occurred. The third gene '-1' or '1' is determination of suction or injection nature of the mass transfer. The next gene (0.0003) quantity is the mass transfer coefficient introduced in Eq. (9) and finally the last variable (2.894) is the inclination angle in radian which its definition is shown in Fig. 2 below.

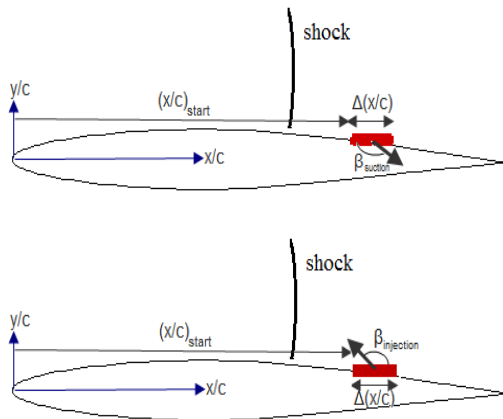


Fig. 2. Definition of suction/injection parameters.

The more crossover probability causes transmission of genetic properties to the next generation, so that the new generation members inherit various gens of their parents. All in all, the present search domain is fully studied by optimization algorithm. By the chromosome length of 5, one crossover would be sufficient. The more mutation probability causes more variety in chromosome generations. So in the present study the mutation is carried out randomly between 1 to 10 times. Disturbance range is used to control and limit mutation operator effects. The disturbance ranges of the mass transfer parameters have been obtained by parametric study (Qin *et al.* 2002). Each chromosome is assessed after reproduction. In fact population assessment determines the GA stop condition which could be reaching the predefined number of iterations or the improvement process of chromosomes. In addition, to determine the level of contribution of each chromosome in the next generation, they should be evaluated by their fitness value.

4. RESULTS

The results obtained by this research are presented in the following section. In the first step the validation of flow solver in the presence of flow control is studied.

4.1 Validation Case

To validate the numerical solution method in turbulent flows, NACA64A010 airfoil is considered that is widely studied by Smith and Walker (1960) in transonic flow with the suction downstream the trailing edge flap hinge line. This airfoil is a 10 percent thick airfoil and if trailing edge flap isn't applied, is a symmetric airfoil. The selected flow condition to validate the obtained results in case of suction is that of 0.5 degree angle of attack, 0.78 Mach number and the Reynolds number of 2.9 million. In this test the suction position has been set at 69 to 72.5 percent of chord length from leading edge which is downstream of the shock wave position without suction application. Suction coefficient is 0.00225 with 1 degree flap deflection. Suction inclination angle is 84 degree related to the airfoil surface and the flow is fully turbulent. The numerical grid is a 195x73 structured grid with the first cell distance of 0.0001 representing the y^+ values of the order of 10 on the airfoil surface and is shown in Fig. 3.

The airfoil lift and drag coefficient sensitivity to grid size are presented in Table 2. The results are an indication of good agreement between the experimental and numerical results for fine and medium grids. In the case of no suction, the lift and drag coefficients are with reasonable accuracy in

Table 2 Investigation of lift and drag coefficients sensitivity to the grid size

Grid Size	With suction		Without suction	
	C_D	C_L	C_D	C_L
155×73	0.01398	0.2007	0.0152	0.2580
195×73	0.01394	0.2012	0.0151	0.2645
235×73	0.01392	0.2016	0.0151	0.2653
195×69	0.0140	0.1923	0.0152	0.2522
195×75	0.01394	0.2043	0.0151	0.2688
Smith and Walker (1960)	0.0130	0.2000	0.0140	0.2400
(Qin <i>et al.</i> 2002)	0.0111	0.2166	0.0138	0.2795

comparison with the numerical results of other references (Qin *et al.* 2002). In the case that the suction is applied, the lift coefficient has higher accuracy.

corresponding to the airfoil with 3 cells located in the suction area show better agreement with the experimental data (Smith and Walker 1960) than the airfoil with only one cell in the suction area.

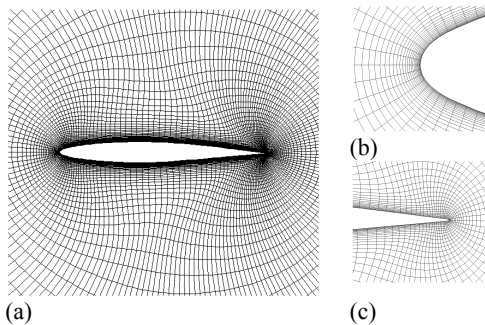


Fig. 3. a) NACA64A010 Hyperbolic grid b) leading-edge zoom b) trailing-edge zoom.

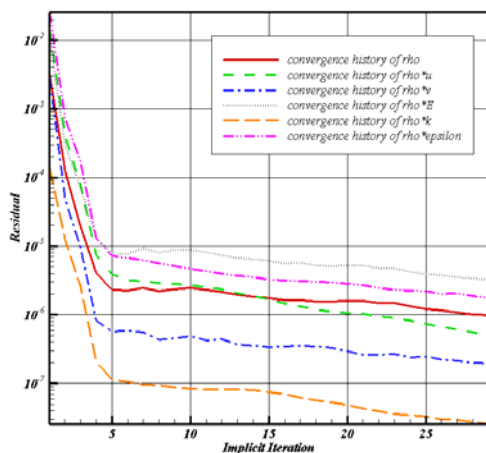


Fig. 4. Convergence history of mean and turbulent flow variables.

The convergence histories of mean and turbulent flow variables are shown in Fig. 4 indicating reasonable level of residual reduction. The surface pressure coefficient distributions with and without the suction are shown in Fig. 5 in comparison with the experimental results. Two sets of results with suction are presented in Fig. 5b while, the results

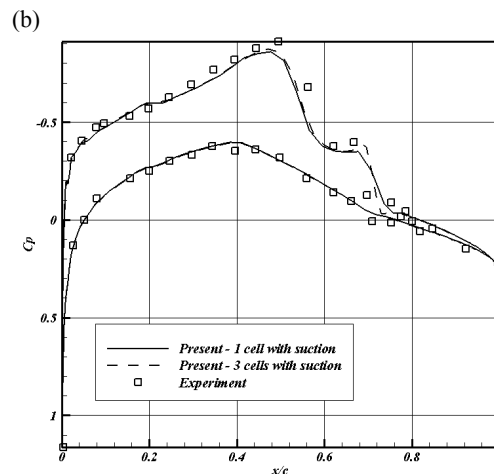
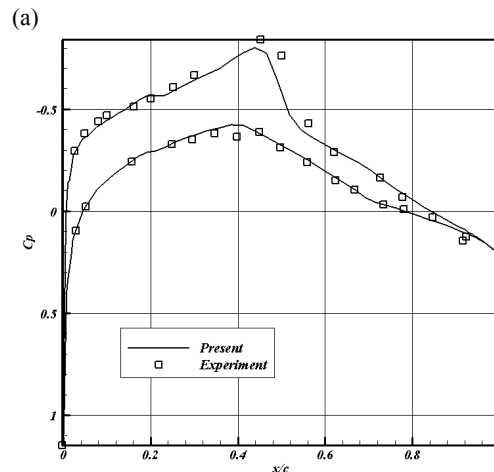


Fig. 5 NACA64A010 surface pressure coefficient distribution a) without suction b) with suction.

Mach number contours with and without surface suction is given in Fig. 6 showing shock strength increase with suction and its movement to the downstream.

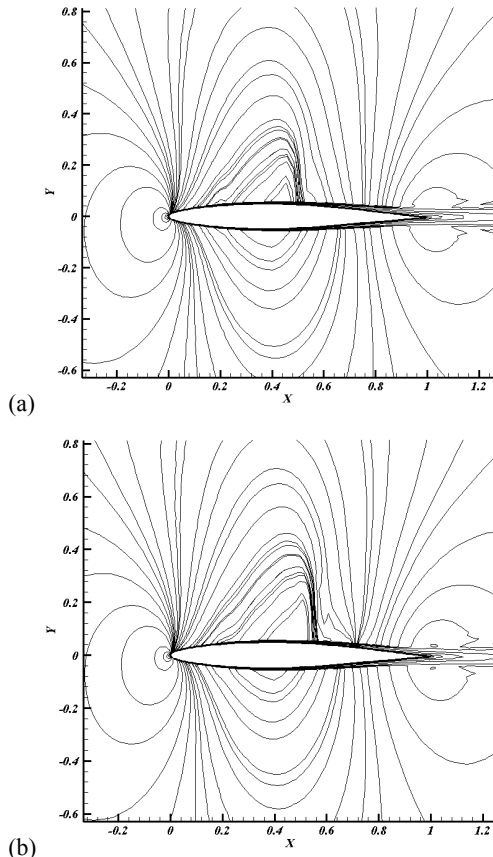


Fig. 6. NACA64A010 Mach number contours a) without suction b) with suction.

4.2 Surface Mass Transfer Optimization

The main purpose of the present work is to show the application of the mass transfer optimization in shock boundary layer interaction control at off-design conditions where the airfoil drag increases suddenly and so its performance deteriorates. In order to demonstrate the effect of the mass transfer on the flow, a well-known test case for NACA64A010 with the Reynolds number of 2.9 million and 0.5 degree angle of attack are selected. Drag divergence diagrams in aforementioned conditions are plotted in Fig. 7.

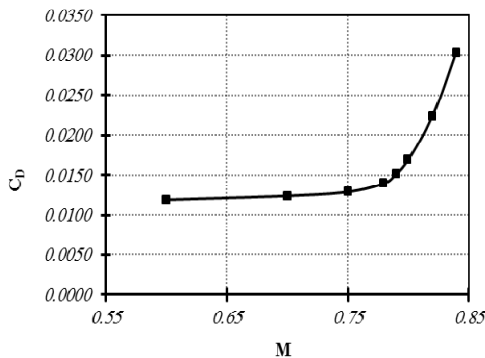


Fig. 7. Drag divergence diagram for NACA64A010 at $Re=2.5 \times 10^6$ and $\alpha=0.5$ deg.

As it can be seen in Fig. 7 the reference Mach number before drag divergence is considered as

0.75. The lift and drag coefficients without suction or injection near and after the drag divergence point are tabulated in Table 3. It is noted that ΔC_D and $\Delta(L/D)$ values are calculated with respect to the reference point. As it can be seen from this table, increasing the Mach number values above the drag divergent will increase the drag coefficients dramatically that leads to more than 30% reduction in aerodynamic efficiency factor.

Table 3 NACA64A010 aerodynamic coefficients in various Mach numbers

M	C_L	C_D	L/D	ΔC_D	$\Delta(L/D)$
0.78	0.200	0.0139	14.41	8.4%	0.6%
0.80	0.213	0.0169	12.62	31.2%	-11.9%
0.82	0.216	0.0223	9.69	73.5%	-32.4%

In order to keep the aerodynamic efficiency of the airfoil at the original cruise level even beyond the drag divergence Mach number, a flow control employment i.e. suction and injection with optimum parameters is required. Optimization process starts with an initial population of chromosomes and their fitness will be measured by fitness function calculation. The fitness functions selected in the present work are aerodynamic performance (lift to drag ratio) and the drag coefficient. In fact, both of these functions are crucial for safe and efficient flight of the aircraft at off-design cruise conditions. Thus, four different objective functions are defined and the optimum results are compared. Each optimization process starts with the selection of the airfoil without surface mass transfer as the first generation and continued to complete 50 generations. Ranges of the surface mass transfer parameters are given in Table 4.

Table 4 Ranges of surface mass transfer parameters variation

Range of variation	Parameters
$C_{Q_{suction}}$	0.0001-0.004
$C_{Q_{injection}}$	0.0001-0.001
β (deg)	10-170
$\Delta(x/c)$	0.027-0.080
$(x/c)_{start}$	0.37-0.80

As it can be seen in this table and it was mentioned earlier, in the present work the injection coefficient level is considered lower than suction one. $\Delta(x/c)$ is the length in which the surface mass transfer will be employed and $(x/c)_{start}$ is the starting position of it.

4.2.1 Optimization Results for Lift to Drag Ratio Maximizing

In the first step, the surface mass transfer parameters are optimized by maximizing the lift to

Table 5 Optimum control parameters values and aerodynamic coefficients for NACA64A010 airfoil with $(L/D)_{max}$ objective function

		Optimization for L/D maximization			Optimization for L/D maximization with C_D considerations	
		M = 0.78	M = 0.80	M = 0.82	M = 0.78	M = 0.80
Optimum parameters	$(x/c)_{start}$	0.64	0.69	0.74	0.42	0.42
	$\Delta(x/c)$	0.053	0.080	0.053	0.027	0.027
	C_q	-0.00379	-0.00372	-0.00361	-0.00379	-0.00379
	β (deg)	164.45	164.64	162.07	170.00	170.00
Aerodynamic coefficients and their variations	C_L	0.2978	0.3462	0.3791	0.2308	0.2504
	C_D	0.0151	0.0215	0.0312	0.0132	0.0169
	L/D	19.689	16.108	12.136	17.500	14.853
	ΔC_L (%)	48.2	62.3	75.2	14.9	17.4
	ΔC_D (%)	8.5	27.2	39.9	-5.4	-0.2
	$\Delta(L/D)$ (%)	36.7	27.6	25.2	21.5	17.7

drag ratio as the objective function. It should however be noted that the value of the drag coefficient may rise during L/D optimization. To prevent drag increment during L/D maximization, the optimization process has also been conducted in a way that the drag coefficient won't exceed its no control value.

In the optimization process, the first generation control parameters are considered as no injection/suction and subsequently the purpose is to find the surface mass transfer parameters so that the aerodynamic performances will be improved. The best members' convergence histories for this case are given in Fig. 8 together with their corresponding drag coefficients. As it can be seen, L/D maximization has been occurred with drag coefficient increase. However, using the extra condition for limiting the drag coefficient, the drag of the best member approximately remains constant or reduces during the evolution.

The Optimum mass transfer parameters and corresponding aerodynamic coefficients are given in Table 5. In this table the values of ΔC_L , ΔC_D and $\Delta(L/D)$ are tabulated relative to the initial condition of no mass transfer application. As it can be observed, the optimum L/D has been achieved by the implementation of the suction on the airfoil surface for both objective functions. It should be noted that the position of the suction is located after the shock wave for the first objective function i.e. $(L/D)_{max}$ while, its optimum place is before the shock wave for the second objective function. However, the higher aerodynamic efficiency factor is achieved by the first objective function. The computational time for optimization process measured on a PC computer with 3.9 GHz speed and after 50 generations, was 20 to 40 hours in average.

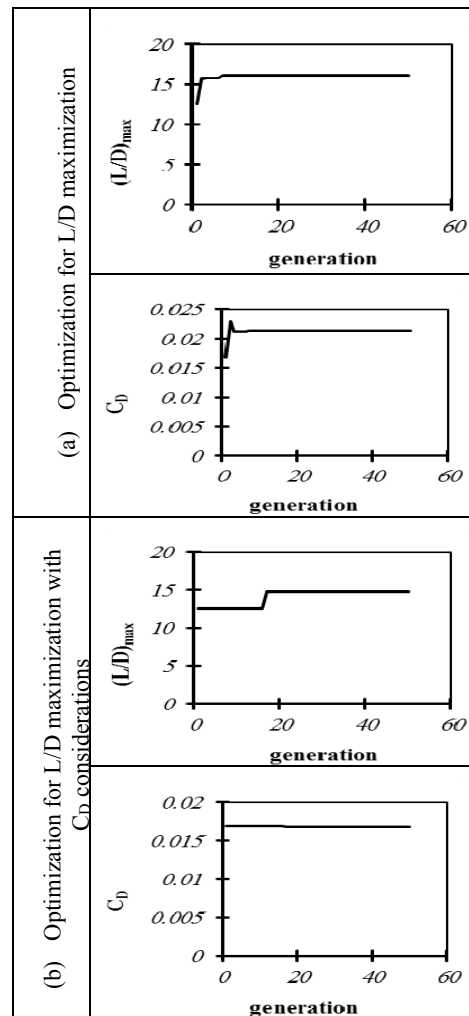


Fig. 8. Optimization convergence histories for NACA64A010 at $(L/D)_{max}$ condition at $M=0.8$.

Table 6. Optimum control parameters values and aerodynamic coefficients for NACA64A010 airfoil at $(C_D)_{min}$ condition

		Optimization for CD minimization			Optimization for CD minimization with L/D consideration	
		M = 0.78	M = 0.80	M = 0.82	M = 0.78	M = 0.82
Optimum parameters	$(x/c)_{start}$	0.74	0.72	0.69	0.42	0.72
	$\Delta(x/c)$	0.071	0.080	0.080	0.027	0.080
	C_Q	0.00090	0.00099	0.00094	-0.00379	0.00059
	β (deg)	162.07	165.54	164.64	170.00	10.49
Aerodynamic coefficients and their variations	C_L	0.1347	0.1341	0.1390	0.2302	0.2156
	C_D	0.0133	0.0151	0.0197	0.0132	0.0221
	L/D	10.094	8.858	7.067	17.460	9.747
	ΔC_L (%)	-32.966	-37.117	-35.752	14.571	-0.392
	ΔC_D (%)	-4.322	-10.380	-11.913	-5.466	-0.981
	$\Delta(L/D)$ (%)	-29.938	-29.834	-27.063	21.472	0.595

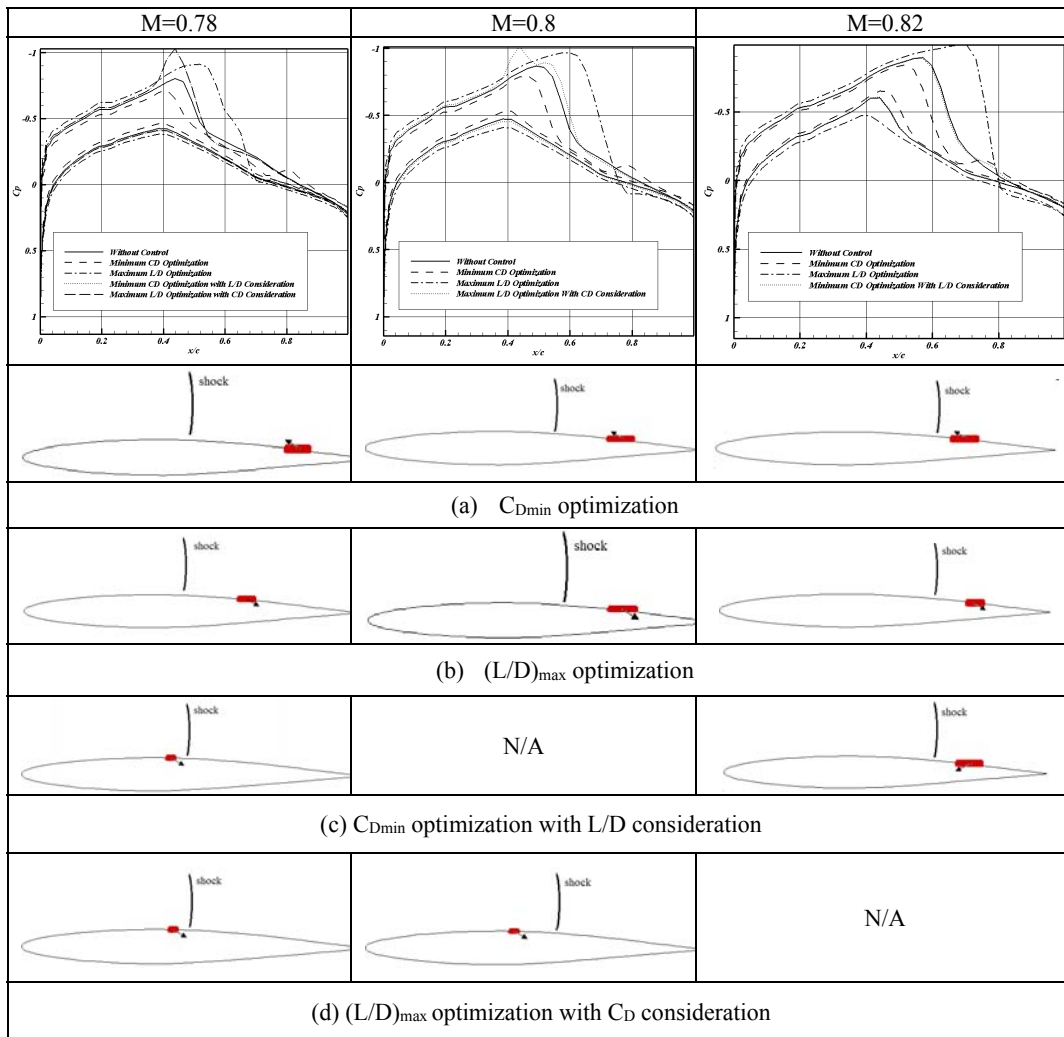


Fig. 9. Optimum results for NACA64A010 airfoil at $Re=2.9 \times 10^6$ and $\alpha=0.5$ deg.

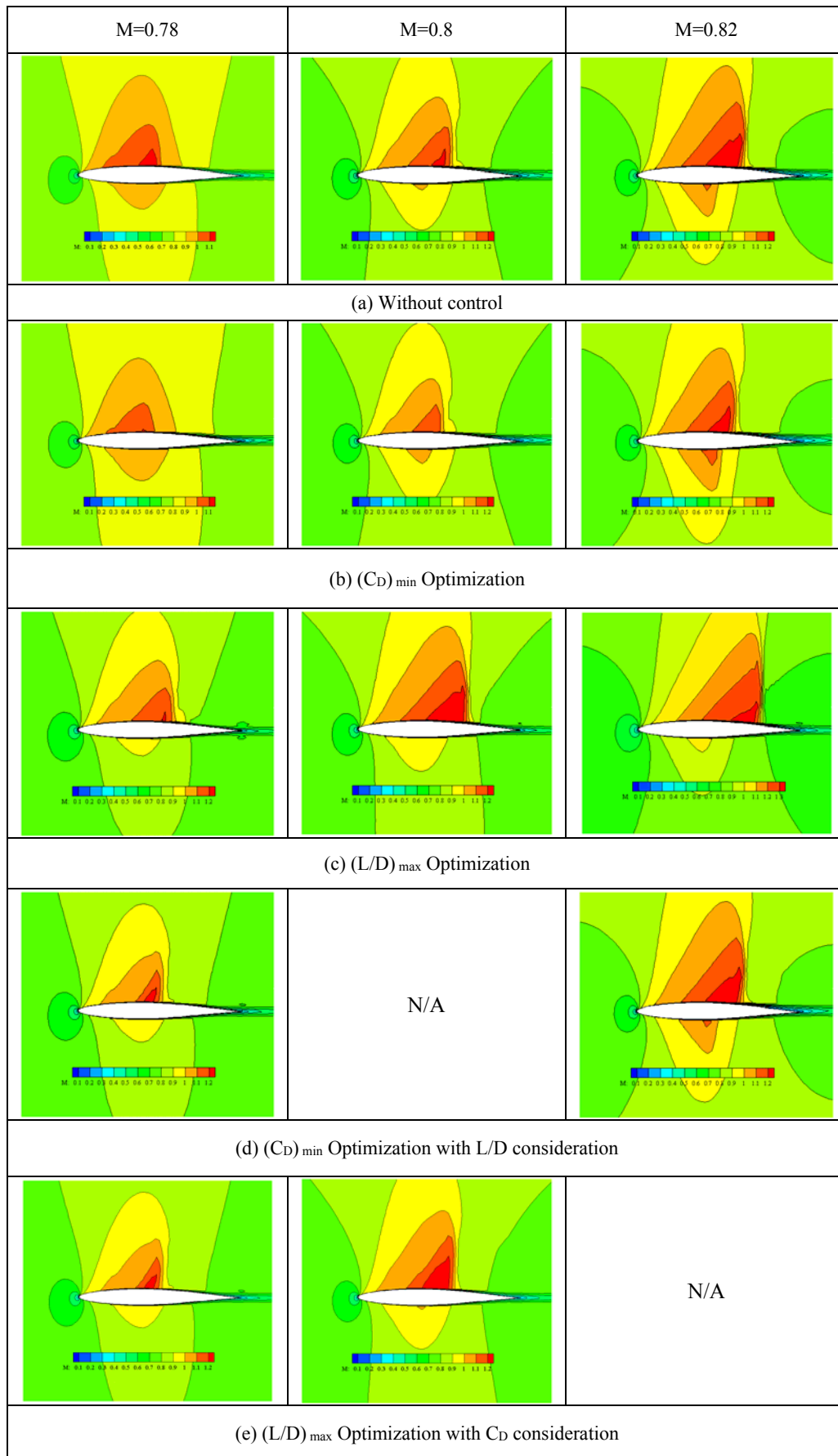


Fig. 10. Mach number contours for NACA64A010 airfoil at $Re=2.9 \times 10^6$ and $\alpha=0.5$ deg.

Table 7. Drag coefficient components for NACA64A010 airfoil with various optimization conditions

	Without control			(L/D) _{max} Optimization			(L/D) _{max} Optimization with C _D consideration	
M	0.78	0.80	0.82	0.78	0.80	0.82	0.78	0.80
C _{D_f}	0.00937	0.00929	0.00916	0.00993	0.00959	0.00963	0.00902	0.00892
C _{D_p}	0.00457	0.00759	0.01317	0.00519	0.01184	0.02141	0.00416	0.00791
ΔC _{D_f} (%)	-	-	-	6.048	3.164	5.098	-3.678	-3.999
ΔC _{D_p} (%)	-	-	-	13.520	55.953	62.553	-9.034	4.191
	Without control			(C _D) _{min} Optimization			(C _D) _{min} Optimization with L/D consideration	
M	0.78	0.80	0.82	0.78	0.80	0.82	0.78	0.82
C _{D_f}	0.00937	0.00929	0.00916	0.00884	0.00871	0.00863	0.00902	0.00875
C _{D_p}	0.00457	0.00759	0.01317	0.00450	0.00641	0.01107	0.00415	0.01332
ΔC _{D_f} (%)	-	-	-	-5.644	-6.309	-5.741	-3.676	-4.466
ΔC _{D_p} (%)	-	-	-	-1.613	-15.544	-15.952	-9.132	1.158

4.2.2 Optimization Results for Drag Minimization

Another objective for mass transfer optimization is drag coefficient minimization. In order to keep the aerodynamic performance at least in the level of its value without flow control the fourth objective function is defined as drag coefficient minimization with limitations on airfoil aerodynamic performance. Results are given in Table 6. It is obvious that the aerodynamic performance is reduced about 30% with drag minimization, but with the fourth objective function its value is increased.

4.3 Discussion

Further investigation about the efficiency of the method is presented in this section. For this purpose, the surface pressure coefficient distributions are plotted in different conditions of no control and with control application using different objective functions. It is obvious in Fig. 9 that the position and the strength of the shock wave play an important role in the final aerodynamic efficiency of the airfoil. The position and the length of the injection or suction holes and the relative strength and inclination of the mass transfer are illustrated in this figure as well. The airfoil drag components are compared in Table 7. A comprehensive comparison of Mach number contours for initial and after optimum control parameters via suction and injection are given in Fig. 9.

Optimization results indicate that to increase the

airfoil aerodynamic performance, the surface suction downstream the shock wave in various Mach numbers is suggested. With increase in flow Mach number, suction location moves more downstream since shock wave location itself moves downstream also and its strength has been magnified with suction. Shock wave location relative to no control condition moves toward trailing edge and its strength and movement is vivid in Mach contours presented in Fig. 10. In addition, since we need stronger suction with Mach increment, the suction location length has been increased with Mach increment. Pressure drag increment with shock wave strength increase is clear in Table 7.

L/D optimization process with considerations of C_D has been led in a way that the suction in 0.78 Mach number is located closer to the shock wave and a bit upstream of it. It can also be seen in Fig. 9 that a sudden increase in shock wave strength is occurred and there is no obvious effect on pressure coefficient plot downstream the shock, so that it prevents skin friction increment. By the observation of airfoil pressure drag change in Table 7, it can be mentioned that suction location has gained in maximum thickness of airfoil so that it has less effect on airfoil pressure drag. In 0.8 Mach number, suction location occurred in similar place where is further from shock wave and upstream of it and since it has no obvious effect on separated downstream boundary layer, there is no remarkable change in shock wave strength and it just results in large pressure reduction locally which can be noticed in Fig. 9. Hence, since suction did not have

any effect on shock wave strength, wave drag does not increase and it prevents total drag increment.

Moreover, flow control optimization results with drag reduction objective for NACA64A010 airfoil indicate injection downstream the shock wave near airfoil trailing edge in all three Mach numbers that with Mach number increase this location moves toward the shock wave position and this injection fairly reduced shock wave strength and moves it upstream which is clear in pressure coefficient distribution in Fig. 9 and Mach number contours in Fig. 10. Mechanism which is warranting flow control with injection near the trailing edge, as it was mentioned in (Qin *et al.*'s 2002), concerns with trailing edge flow improvement which is similar to a jet flap that increases flow circulation in trailing edge. Drag coefficient minimization results with condition of no aerodynamic performance loss moves toward selection of suction method since injection causes loss in aerodynamic performance in almost all cases.

5. CONCLUSIONS

In this paper, a dual-time implicit finite volume solver has been employed to be improved and prepared to apply airfoil surface mass transfer boundary condition. Then by the validation of its results in no control case and in presence of that, an optimization process of suction/injection parameters has been performed. Genetic Algorithm optimization method has been selected due to its high ability to find global optimums. It was concluded that the optimization results of surface mass transfer flow control are very sensitive to flow condition. To increase an airfoil aerodynamic performance in drag divergence condition, most of the results were an indication of suction power to fulfill our desire objective and it should be applied downstream the shock wave. More over if the designer would tend to reduce airfoil drag in drag divergence condition, the optimum flow control condition would be the employment of injection upstream the shock wave. Although the aforementioned points are too general to design a flow control system, by the optimization procedure of this study, these flow control parameters such as location, length, angle and whether mass transfer should be applied as suction or injection has been determined more specifically.

REFERENCES

- Anderson, W. K. and D. L. Bonhaus (1999). Airfoil design on unstructured grids for turbulent flow. *AIAA Journal* 37(2), 185-191.
- Babinsky, H. and J. K. Harvey (2011). *Shock Wave-Boundary-Layer Interactions*. Cambridge University Press.
- Cook, P. H., M. A. McDonald and M. C. P. Firmin (1979). Aerofoil RAE 2822 pressure distribution and boundary layer and wake measurements.
- Deb, K. (2001). *Multi-objective optimization using evolutionary algorithms*. John Wiley and Sons, Chichester, UK.
- Delery, J. M. (1999). Shock phenomena in high speed aerodynamics: still a source of major concern. *The Aeronautical Journal* 103(1019), 19-34.
- Goldberg, D. E. (1989). *Genetic Algorithm in Search, Optimization and Machine Learning*. Addison-Wesley, Massachusetts:
- Jahangirian, A. and A. Shahrokhi (2009). Inverse design of transonic airfoils using genetic algorithm and a new parametric shape method. *Inverse Problems in Science and Engineering* 17(5), 681-699.
- Jahangirian, A. and A. Shahrokhi (2011). Aerodynamic shape optimization using efficient evolutionary algorithms and unstructured CFD solver. *Computers and Fluids* 46, 270-276.
- Jahangirian, A. and M. Hadidoolabi (2005). Unstructured moving grids for implicit calculation of unsteady compressible viscous flows. *International Journal for Numerical Methods in Fluids* 47 (10-11), 1107-1113.
- Khoshkhou, R. and A. Jahangirian (2016). Numerical simulation of flow separation control using multiple DBD plasma actuators. *Journal of Applied Fluid Mechanics* 9 (4), 1865-1875.
- Lauder, B. E and D. B. Spalding (1974). The Numerical computation of turbulent flows. *Computer Methods in Applied Mechanics and Engineering* 3, 269-289.
- Marco, N. and S. Lanteri (2000). A Two-Level Parallelization strategy for genetic algorithm applied to optimum shape design. *Journal of Parallel Computing* 26, 377-397.
- Mazaheri, K. and A. Nejati (2016). The multi-point optimization of shock control bump with constant-Lift constraint enhanced with suction and blowing for a supercritical airfoil. *Flow, Turbulence and Combustion* 96(3), 639-666.
- Obayashi, S. and T. Tsukahara (1997). Comparison of optimization algorithm for aerodynamic shape design. *AIAA Journal* 35(8), 1413-1415.
- Oyama, A., S. Obayashi and T. Nakamura (2001). Real-coded adaptive range genetic algorithm applied to transonic wing optimization. *Applied Soft Computing* 1, 179-187.
- Pehlivanoglu, V. and B. Yagiz, (2012). Aerodynamic design prediction using surrogate-based modeling in genetic algorithm architecture. *Aerospace Science and Technology* 23, 479-491.
- Qin, N., Y. Zhu and D. I. A. Poll (1998). Surface suction on aerofoil aerodynamic characteristics at transonic speeds. In *Proceedings of the Institution of Mechanical Engineers, Part G*:

- Journal of Aerospace Engineering* 212, 339-351.
- Qin, N., Y. Zhu and S. T. Shaw (2002). Numerical study of active shock control for transonic aerodynamics. *International Journal of Numerical Methods for Heat and Fluid Flow* 14(4), 444-466.
- Shahrokhi, A. and A. Jahangirian (2010). A surrogate assisted evolutionary optimization method with application to the transonic airfoil design. *Engineering Optimization* 42(6), 497-515.
- Smith, D. W. and J. H. Walker (1960). *Test of an Area Suction Flap on a NACA64A010 Airfoil at High Subsonic Speeds*, NASA TN D 310.
- Stanewsky, E., J. Delery, J. Fulker and P. de Matteis (2002). *Drag reduction by shock and boundary layer control, (results of project EUROSHOCK II supported by the European Union 1996-1999)*. Springer, Heidelberg.
- Stolcis L. and L. J. Johnston (1990). Solution of Euler equations on unstructured grids for two dimensional compressible flows. *Aeronaut. J.* 94(936), 181-195.
- Thompson, J. F., B. K. Soni and N. P. Weatherill (1999). *Handbook of Grid Generation*. CRC Press LLC.
- Wong, W. F. (1977). Application of Boundary Layer Blowing to Suppress Strong Shock Induced Separation in a Supersonic Inlet. *AIAA 15th Aerospace Sciences Meeting* 77-147.
- Yagiz, B. and O. Kandil, (2009). Optimization of active flow control in transonic aerodynamics. In *proceeding of 27th AIAA Applied Aerodynamics Conference*.
- Yagiz, B., O. Kandil and V. Pehlivanoglu (2012). Drag minimization using active and passive flow control techniques. *Aerospace Science and Technology* 17, 21-31.
- Zhang, F., S. Chen and M. Khalid (2002). Optimization of airfoils and wing using genetic algorithm. In *Proceeding of ICAS2002 Conference*.